ACS APPLIED MATERIALS & INTERFACES

Applications of Polymer, Composite, and Coating Materials

Lightweight Porous Polystyrene with High Thermal Conductivity by Constructing 3D Interconnected Network of Boron Nitride Nanosheets

Wenying Zhou, Yong Zhang, Jianjun Wang, He Li, Wenhan Xu, Bo Li, Long-Qing Chen, and Qing Wang

ACS Appl. Mater. Interfaces, **Just Accepted Manuscript** • DOI: 10.1021/acsami.0c11543 • Publication Date (Web): 17 Sep 2020

is published by the American Chemical Society. 1155 Sixteenth Street N.W., Washington, DC 20036

Lightweight Porous Polystyrene with High Thermal Conductivity by Constructing 3D Interconnected Network of Boron Nitride Nanosheets

Wenying Zhou[a,b,c], Yong Zhang[a], Jianjun Wang[a], He Li[a], Wenhan Xu[a], Bo Li[d], Longqing Chen[a], Qing Wang[a*]

[a]*Department of Materials Science and Engineering, Pennsylvania State University, University Park, Pennsylvania 16802, United States*

[b]*School of Chemistry and Chemical Engineering, Xi'an University of Science & Technology, Xi'an, 710054, China*

[c]*Key Laboratory of Engineering Dielectrics and Its Application, Ministry of Education, Harbin University of Science and Technology, Harbin, 150080, China*

[d]*Poly K Technologies Co., State College, Pennsylvania 16803, United States*

ABSTRACT: A composite foam consisting of foamed cross-linking polystyrene (*c*-PS) and boron nitride nanosheets (BNNSs) was synthesized, which shows a higher thermal conductivity (TC) than the corresponding solid counterparts. The BNNSs fillers are found to be aligned along the cell wall as a result of the biaxial stress field from cell expansion during the formation of 3-dimensional interconnectivity in the foams, resulting in an enhanced TC of 1.28 W/m K, near 2 and 4 times those of its solid counterpart and pure *c*-PS, respectively. It is found that the foaming-assisted formation of the filler network is an efficient strategy to improve the TC at low filler loadings in the composites. Furthermore, the composite foams exhibit low-density, rather low dielectric constants and dissipation factors at wide frequency and temperature ranges. The present work provides a novel approach to designing and preparing lightweight heat conductive polymers with low filler loadings as low-density heat management materials for potential applications in aeronautics and aerospace components.

Keywords: *Thermal conductivity, Polymer composites, Porous structure, Boron nitride nanosheets, Dielectric properties*

1. INTRODUCTION

The rapid development of electronics and optoelectronics such as high-power microelectronic packaging devices, LED (light emitting diode) lighting and chip encapsulation toward high speed and high-performance has demands placed on heat removal.[1-3] Therefore, the effective thermal management is critically important to ensure system performance and reliability, and enhance lifetime and accuracy.[4-6] Compared to traditional thermally conductive materials such as metal, carbon and ceramics materials, polymers have poor thermal conductivity (TC, ranging from 0.1~0.3 W/m K) because of random structures and twisting chains. However, polymers, due to their various advantages including low cost, lightweight, and easy processability, are becoming increasingly popular in heat-intensive applications such as LED housing, cell phone casting, electronic chip encapsulation, and high-power electric motor where heat accumulation can have deleterious effects.[2-4] These applications, along with emerging technologies such as flexible or wearable electronics, for which the requirements on mechanical flexibility and lightweight cannot be met by most conventional thermal management materials, put strong technological incentives on developing heat conductive polymers to avoid overheat in encapsulated chips or microelectronic packaging devices working under high frequencies or high voltages.[7-12]

Aligning the polymer chains represents an approach to achieving high TC in polymers. However, this approach requires certain fabrication techniques, such as electrospinning, nanoscale templating, mechanical stretching,[13-17] and the TC in these aligned polymers are only limited to the direction of chain orientation. It is quite challenging to take advantage of a single polymer chain in bulk structure to obtain high intrinsic TC polymers. Blending with high TC fillers is the most commonly used approach to enhancing TC of polymers, which can yield the values of TC ranging

from 1 to 10 W/m K.[18-24] However, the large amount of fillers (≥ 65 wt% fillers such as AlN, Si_3N_4, Al_2O_3, BN or SiC) required to achieve appreciable enhancement in TC not only significantly increases the material weight and cost but also leads to undesired electrical, mechanical, and optical properties, or loss of the easy processability generally associated with polymers.[20-23] Therefore, it is essential to develop new design and fabrication strategies of heat conductive polymer composites loaded with minimum filler contents.

When the TC ratio of the filler to the polymer exceeds 1000, further increasing the TC of filler has negligible effect on the effective TC of the composites.[24] Therefore, the inclusion of CNT (carbon nanotube) or graphene flake with extremely high TC in polymers failed to remarkably increase the TC of the polymers owing to the large thermal interfacial resistance resulting from the significant phonon scattering at the interfacs[25-28] due to the unpaired phonon frequency.[6, 9, 10, 12, 29-35] In order to circumvent this challenge and decrease the thermal interfacial resistance, a 3-dimension (3D) network of fillers in the matrix has recently been developed.[8, 12, 36-42] Other strategies include electric or magnetic field induced filler alignment, ultra-drawing, frozen-drying, and ultra-sonication, etc.[43-49]

Up to now, extensive investigations on the preparation of heat conductive composites have been carried out on solid polymer matrix.[1, 5, 18-32] The porous polymers with low densities and reduced weights, although they are promising for applications that are sensitive to weights such as aeronautics and astronautics, have received much less attention due to their extremely low TC as a result of introduced air (i.e. 0.024 W/m K). Herein, we report the preparation and characterization of the porous polymer composites with high TC and low mass density when compared to their solid counterparts.

It was reported that foaming-induced biaxial flow could align filler particles along the cell

boundary and enhance the formation of 3D network of fillers in polymer and therefore result in the improvement in the mechanical, electrical and/or thermal properties of materials and simultaneous suppression of the cell rupture.[31, 50-52] For filled polymer foams, on the one hand, TC will decrease due to the introduction of air in matrix. On the other hand, the foaming-induced filler alignment around expanding bubbles will enhance the formation of 3D filler networks, thereby leading to rapid increase in TC. Therefore, the final TC depends on these two competing effects. Thus, foamed polymers with enahnced TC could be achieved at optimal volume expansion (VE) percentage and filler content. In this work, the boron nitride nanosheets (BNNSs)/cross-linked polystyrene (*c*-PS) composites were prepared and foamed by using purified water as a foaming agent at a certain temperature in confined space. The effects of filler loading, particle size and dstribution, and VE percentage on TC and dielectric properties of composites have been investigated. The obtained structure-to-property relationships would provide guidelines to develop ultralow density polymers with enhanced TC.[52]

2. EXPERIMENT SECTION

2.1. Materials

Preparation of BNNSs: Typically, 8 *g* h-BN powders (Sigma-Aldrich) were dispersed in 400 *ml* Dimethylformamide (DMF) (Sigma-Aldrich) under vigorous stirring. The mixture was then subjected to a 96 h tip-type sonication (175 W, 500 W×30%). The resultant mixture was first centrifuged at 3500 rpm for 15 minutes, and the supernatant was collected. This step purified the mixture from unexfoliated h-BN powders. Then, the supernatant was subjected to a 30-minutes centrifugation at 10000 rpm to precipitate BNNSs. After vacuum drying overnight at 80 ^{o}C, BNNSs were obtained.

2.2. Preparations of BNNSs/c-PS foam

Preparation of BNNS/c-PS foam: a 20 *ml* slender glass bottle was loaded with 0.82 *g* purified styrene (Sigma-Aldrich, 99%), 0.0082 *g* 2, 2'-azobis(2-methylpropionitrile) (Sigma-Aldrich, 99%), 0.21 *g* divinylbenzene (Aldrich, 80%) purified with 0.2 *M* NaOH (Sigma-Aldrich), 0.037 *g* span-80 (Sigma-Aldrich), and a stir bar. The contents were then mixed for about 30 minutes on a stir plate. After that, different content of purified water was added to the mixture dropwisely with stirring. The final mixture was stirred on a stir plate for 1 h. Next, various loading of BNNSs nanoparticles was added to the solution, then the mixture was ultrasoniced for 30 min, and then stirred for 24 h. The contents were sealed and placed into an oven at 60 ^{o}C for 24 h to finish the styrene' polymerization and crosslinking reactions. The bottle was then broken to remove the foamed sample, and it was then placed in the same oven for another 48 h until dry. The same procedures were applied to fabricate both solid and foamed composites to ensure all samples experiencing the same thermal history. For solid samples, no water was used in the mixture. The preparation procedures of the composite foams is illustrated in **Figure 1**.

The VE percentage of a foam is defined in Equation (1):

$$VE\% = (\frac{V_{foam} - V_{solid}}{V_{solid}}) \times 100\% \quad (1)$$

where, V_{foam} is the volume of polymer foams, and V_{solid} is the volume of solid samples.

In this work, the V_{foam} is closely related with the water loading, i.e., it increases with the content of water. Thus, a desired VE value can be obtained through calculating and controlling the water loading in the sealed bottle. Since the VE percentage of the composite foam is sensitive to the composition of the water, so, TC of the composites can be effectively tuned by adjusting the water concentration.

2.3 Characterization

A scanning electron microscope (SEM, JEM-7000F, JEOL, Japan) and a field emission scanning electron microscope (FESEM, JEM-6700F, JEOL, Japan) were used to observe the microstructures in the composite samples. All samples were broken and the fractured surfaces were sputtered with a thin layer of gold to prevent charge accumulation prior to observation. A TCi Hot Disk thermal analyzer (C-Thermal, Canada) was used to measure TC of the samples using the modulated transient place source method, which is based on a transient technique.

The temperature of the composites was recorded by an infrared thermograph (Fotric 220, China). The dielectric constant and loss were measured using an Agilent LCR meter (E4980A). Silver electrodes of a diameter of 20 mm were pasted on both sides of the samples (~3 mm) for all the electrical measurements. The temperature dependences of the dielectric constant and dissipation factor were analyzed with the frequency ranging from 10^2 Hz to 10^6 Hz and over a broad temperature range 25-180 ^oC with a Hewlett Packard 4284LCR meter using a 2 V bias in conjunction with a Delta Design oven model 2300 equipped with liquid nitrogen cooling system.

3. Results and discussion

3.1 Effects of filler loading and VE on thermal conductivity.

Figure 2a presents the effect of BNNSs loading on TCs of the solid and foamed polymer composites with a VE of 45% and 92%, respectively. TC increases with the filler loading ranging from 0 to 30 wt% for the solid and foamed composites. At low filler loadings, the amount of BNNSs is not sufficient to establish a heat conductive network in the matrix. Thus, TC increases rather slowly owing to enormous thermal interfacial resistance resulting from phonon scattering at the interfaces, which is detrimental to heat conduction.[1] With further increase of the filler content, BNNSs are able to form an interconnected network in the matrix. Consequently, the corresponding TC increases rapidly at high filler loadings, i.e., 30 wt%. At low filler loadings, TC of the foamed

polymer composites is obviously lower than that of solid counterparts because of the introduction of air voids with ultralow TC into the matrix. With increasing filler content, the TC of foamed polymer composites begin to approach and exceed that of solid samples. For example, at 30 wt% filler loading, the maximum TC of the foamed polymer composites reach 1.28 W/m K, vs. 0.65 W/m K of the solid composites with the same filler loading. A more than 97% enhancement in TC of the foamed sample is appartantly attributed to the formation of interconnected network of BNNSs in the matrix.[4-9]

Figure 2b indicates that the VE has prominent influence on TC of the composites. The three samples with various filler loadings exhibit similar behaviors in TC, i.e., TC first decreases, and then increases to the maximum value with VE before it continues to decrease to a very low value. For example, at 30 wt% BNNSs loading, and a VE of 45%, the highest TC of 1.28 W/m K is obtained.. Our results suggest that the TC of the foamed composites mainly depends on the filler loading and VE, and can exceed that of its solid counterpart at certain conditions. Thus, TC of the foamed composites can be effectively tuned by controlling VE when the filler loading is greater than the critical content.

Figure S1 (supporting information) describes the dependence of TC of the foamed composites on the VE and filler loading. For the solid BNNSs/*c*-PS at a relatively low filler loadings, i.e., 30 wt%, the particles were randomly dispersed in the matrix, and no interconnected network of fillers for heat flow could be established in the matrix. Phonon propagations are significantly hindered and suppressed because of phonon scattering at the interfacial boundary between the filler and the matrix, thereby leading to low TC.[1, 43-47] For the foamed polymer composites, apparently, due to the biaxial flow of materials during the foaming process, the BNNSs probably either turn their face fixed face orientation, or are aligned along the flow direction of materials, i.e., along the cell

boundary. Therefore, the preferential orientation of BNNS platelets along the cell wall of expanded void cell would promote the interconnectivity of BNNSs, leading to a favorable impact on TC of the composites owing to the established 3D pathways for phonons transfer.[39, 53] Compared with the solid samples, under the same filler loading, it is the presence of foaming-induced filler alignment that promotes the formation of 3D heat conductive network of BNNSs in *c*-PS,[54] which significantly reduces the thermal interfacial resistance, and builds up the highway for phonon propagation across the composites, also illustrated schematically in **Figure 2**c. Therefore, TCs of the foamed polymer composites at moderate VE values are much higher than those of their solid counterparts.

As evidenced in **Figure 2**(a-b) and **Figure S1**, the foaming-induced biaxial stress field increases with bubble expansion, thereby resulting in a higher degree of filler alignment along the cell wall to establish a thermally conductive network. However, at a low VE, the filler particles are too isolated to form interconnected networks for phonon propagation, thus resulting in high thermal interfacial resistance in the composites. Moreover, the introduction of thermal insulating air (i.e. 0.024 W/m K) further significantly reduces the TC of the foamed composites compared with their solid counterparts. As the VE increases, the foaming-induced alignment of BNNSs in the *c*-PS matrix along the cell wall results in a higher probability of filler networking.[55-57] Once the cell expansion reaches the critical level, i.e., most filler particles become preferentially aligned around the expanded cell wall, the TC reaches the maximum value (as seen in **Figure 2**c). With further increasing VE, excessive volume expansion would disrupt the interconnected thermally conductive network of the fillers that are already established, resulting in a high thermal interfacial resistance in the composites. The introduction of a large amount of thermal insulating voids into the matrix becomes the predominant adverse factor on the TC of the foam.[31]

Similarly, at a moderate VE and a low filler loading, the filler particles are unable to form

interconnected networks because of the insufficient amount of filler. Thus, the phonon scattering at the interface are prominent and remarkably suppresses the phonon transfer and shorten the phonon mean free path, resulting in depressed heat conduction.[35-39] Therefore, the different impacts of VE on the TC of the foamed composites indicates that cell expansion-induced effect is more significant in the composite foams with relatively low VE values. The mound-shape TC-VE relationship from **Figure 2**b reveals that there are two or more competing factors governing the TC of the composite foams. Overall, the positive effects of foaming on the TC of the foamed polymer include: 1) foaming-assisted filler alignment along the cell walls, and 2) localization of BNNSs in the solid phase of the foam *c*-PS. The negative influences of foaming on the TC includes: 1) the introduction of thermally insulating voids in the matrix, and 2) the disruption of filler network between adjacent cells.[31, 35,47, 52]

Figure S2 (supporting information) summarizes the TCs of the composites filled with BNNSs with different sizes (lateral size of 1 μm and 0.5 μm, respectively). In **Figure S2**a, the particle size shows negligible influence on the TC of th ecomposite foam at low filler loadings because the population density of BNNSs is not sufficient to form interconnected networks for heat flow. Therefore, the TC depends more siginificantly on the filler concentration. The composites with a smaller BNNSs demonstrates more pronounced enhancement in the TC compared to those with a larger filler.[1] This is because the smaller particles with a higher specific surface area would have a higher efficiency to form robust and stable heat conductive pathways/networks at higher filler loadings in the matrix.[3, 5] As shown in **Figure S2**b, only at moderate VE values, the composites with smaller particles increases more quickly with filler loading.[22-26, 31] However, at low and high VE values, the particle size has negligible influence on the TC of the composites because there is no network formed at these stages. Therefore, the filler size could influence the TC only when an

interconnected network of the particles is formed in the composites.

3.2 Effective filler loading

Effective filler loading in the foamed polymers can be determined by the equation:[31]

$$V_e = \frac{V_f(V_{solid}+V_{void})}{V_{void}} \times 100\% \quad (2)$$

where, V_e is the effective filler loading, V_f is the volume fraction of filler in the composites, V_{solid} is the volume of the solid phase in the foamed composites, and V_{void} is the total volume of all voids in the foamed composites.

According to Equation 2, the effective filler loadings for different systems are plotted in **Figure 2**d, which presents the effect of VE on the effective filler loading in solid phase. With the increase of VE, the effective filler loading exhibits a linear increase, which could result in a higher probability of filler networking, thereby enhancing the TC of the foamed composites. For instance, a 45% VE of *c*-PS foam with 15.8 vol% BNNSs results in an effective BNNSs concentration of 18.7 vol%. The localization of BNNSs in the *c*-PS matrix would result in a higher probability of filler networking, thereby improving the TC of the composite foams.

It is well known than the TC is closely related with the microstructure of foamed composites. Apart from the VE, the cell size has a prominent effect on composites' microstructure, thereby influencing the TC and other physical properties. **Figure S3** (supporting information) presents the TC dependence on cell size for the composites at various filler loadings and VE values. **Figure S3**a depicts the TC of c-PS with 20 wt% and 30 wt% BNNSs and controlled VE against cell size. TC is seen to first increase to a maximum value, then decrease with further incrresing VE, and the maximum TC is obtained at a moderate VE for different systems. TC can be enhanced by a moderate amount of cell size growth, while, high VE, i.e., excessive cell expansion, will bring about

suppressed TC. For 30 wt% BNNSs/c-PS, the top TC is observed to shift towards higher VE, and the best cell size for the three foamed composites with a VE of 22%, 45% and 92%, are 6μm, 8μm and 18μm, respectively. Similiarly, the 20 wt% BNNSs/c-PS exhibit similar TC trend with cell size distribution. At low VE value cell size has important effect on TC of composites, whereas, TC is insensitive to the variant of cell size at high VE.[1, 31] As the cell size further increases, both excess foam expansion and cell size growth would disrupt the formed filler interconnectivity among the cell walls, thereby reducing the TC owing to the introduction of large volume of thermally insulating. So, the different in sensitivity of TC on cell size implies that cell expansion induced effects are more significant in foamed composites with high filler concentration and low VE.[31, 47, 52] **Figure S3**b plotts the calculated average cell size as a function of VE for c-PS with 20 wt% and 30 wt% of BNNSs. Cell size is seen to increase with VE for the two composites. And the maximum TC is achieved at a VE of 45% for 30 wt% BNNSs/c-PS composites, the optimal cell size is about 6 μm, which is consistent with the results in **Figure 2**b and **Figure S3**b.

From Figure S3, it is found that there exsits relationship between the VE and filler loading, which causes the change to the microstructure of foamed composites, thereby inflencig TC of composites. At low filler loading, no matter how to alter the VE value, TC changes little against both VE and cell size. The cell size of a foam increases almost linearly with the VE, so, at large VE or cell size, the fillers can not be connected with each, thus producing margin enhancement in TC of samples owing to the large thermal contact resistance. Only at relatively high filler loading, the cell size is seen to play an obvious effect on TC. So, TC is closely with the microsture of samples. with increasing the filler loading, BNNSs begin to contact with an increase in VE and cell size, and the network can be fromed at an optimal VE value corresponding to the best cell size, thereby producing the maximum TC, which can not be obtained for the other canses such as the VE = 0 or

92%. Therefore, in order to obtain a maximum TC, the microstructure with connected BNNSs inside the cell wall should be created and developed by virture of adjusting the VE, filler loading and cell size parameters.

3.3 Simulation results

The thermal transport process in the composite can be obtained by solving the heat conduction equation:

$$\frac{\partial}{\partial x_i}\left[k_{ij}(\mathbf{x})\frac{\partial T(\mathbf{x})}{\partial x_j}\right]+q(\mathbf{x})=\rho(\mathbf{x})c_{\mathrm{p}}(\mathbf{x})\frac{\partial T(\mathbf{x})}{\partial t} \quad (3)$$

where $k_{ij}(\mathbf{x})$, $\rho(\mathbf{x})$, $c_{\mathrm{p}}(\mathbf{x})$, and $T(\mathbf{x})$ represent the spatial dependent TC tensor, mass density, constant-pressure heat capacity, and temperature. For the TC, istropic values of 0.2, 350, and 0.024 W/m K are assigned for the polymer phase, BNNSs phase, and pore phase, respectively. The densities of the polymer phase, BNNSs phase, and pore phase are assumed as 1.0 g/cm^3, 2.1 g/cm^3, 0.0012 g/cm^3, respectively. Heat capacities of 1.3 J/(g K), 0.793 J/(g K), and 0.718 J/(g K) are used for the polymer phase, BNNSs phase, and pore phase, respectively. For the composite with a specific microstructure, the temperature distribution $T(\mathbf{x})$ and heat flux J_i at the steady state of Equation 3 are solved using the phase-field Spectral Iterative Perturbation Method,[56, 59] from which the effective TC can be calculated according to $k_{ij}^{\mathrm{eff}}=-\langle J_i\rangle/\langle\partial T(\mathbf{x})/\partial x_j\rangle$ with $\langle\ \rangle$ representing the volumetric average.

Figure 3 depicts the several microstructure models of BNNSs/*c*-PS with various VE and the simulation results of their effective TCs and energy flux distributions. With expanding the total volume of the samples, the volume fraction of pores increases and the volume fraction of BNNSs decreases. When the expanded volume is about 111% times of the pristine sample, BNNSs are dispersed in *c*-PS matrix. The effective TC decreases to be around 0.26 W/m K as a result of the introduced pores. With continuous increase of the total volume to 146% times of the pristine sample,

more micro-pores are introduced and BNNSs are driven to be around the pore surfaces. As a result, BNNSs are connected with each other to form a continuous shell layer during the foaming process. The connection of the shell layers makes a continuous path for conducting thermal energy, which can be seen from the thermal energy flux distributions. However, with expanding the volume to be, e.g. 373% times of the pristine sample, the total volume fraction of BNNSs becomes very small (i.e. 2.68%). In this case, BNNSs are unable to form continuous thermal conductive path and only randomly dispersed around the pore walls. Therefore, the effective TC of the excessively expanded sample will be even much smaller than the pristine sample. The simulation results shown in **Figure 3** agree well with the experimental data as shown in **Figure 2**b.

3.4 Heat dissipation performance

In order to demonstrate the thermal management applications of the BNNSs/*c*-PS porous composites, the variations of surface temperature of the composites with time during cooling were recorded by an infrared thermal imager. The samples of pure *c*-PS, 30 wt% BNNSs/*c*-PS solid composites (VE=0), 25 wt% BNNSs/*c*-PS (VE=45%) and 30 wt% BNNSs/*c*-PS (VE=45%) composites were employed. The variantion of surface temperature with cooling time for the four systems were measured from the same initial temperature. The images of temperature distribution with time are shown in **Figure 4**. To investigate heat dissipation performance, all the samples were placed in an oven with a temperature of 75 ^{o}C for 3 h to ensure uniform sample temperature and then transferred to a thermal insulating foam stage at room temperature. As shown in **Figure 4**a, during the heat dissipation process, the samples of 25 wt% BNNSs/*c*-PS (VE=45%), and 30 wt% BNNSs/*c*-PS (VE=45%) composites exhibit much faster decrease with time in comparison with the pure *c*-PS and 30 wt% BNNSs/*c*-PS solid composites containing randomly dispersed BNNSs. This is because the composites of 25 wt% BNNSs/*c*-PS (VE=45%), and 30 wt% BNNSs/*c*-PS (VE=45%)

have much better thermal responses due to their higher TC. Taking the sample surface temperature at 300 *s* as an example, they are about 19 °C and 23 °C for the 30 wt% BNNSs/*c*-PS (VE=45%), and 25 wt% BNNSs/*c*-PS (VE=45%) composites, which are lower in comparison with the composites of pure *c*-PS (34 °C) and solid 27 wt% BNNSs/*c*-PS (30 °C). From the infrared thermal images of the four systems shown in **Figure 4**b, it is clearly observed that the results of surface temperature variation are consistent of those shown in **Figure 4**. These results illustrate that the prepared BNNSs/*c*-PS foams at moderate VE are promising for applications in novel lightweight thermal management materials.

3.5 Microstructures

Figure 5 presents the representive SEM micrographs of the BNNSs/*c*-PS composits filled with different filler loadings. As shown in **Figure 5**a, the filler partciles were homogeneously dispersed in the matrix of the 30 wt% BNNSs/*c*-PS solid composites (VE=0%). As a result, no heat conductive pathways are formed in the matrix, which accounts for the slow enhancement in the TC of the composites with filler loading. **Figure 5**(b-d) illustrates the microstructures of the 25 wt% and 30 wt% BNNSs/*c*-PS composits with a VE of 45%. It is found that the BNNSs were preferentially aligned around cell wall in the fomed composites and able to form a interconnected heat conductive network for phonon transfer.[32, 36] Compared with the random dispersion of BNNSs in the matrix (**Figure 5**a), at the same filler loading, VE generates biaxial stretching along their cell walls, and therefore induces the preferencial alignment of the platelets along the cell walls. Consequently, the localization of BNNSs in the matrix results in a higher probability of filler networking, and thus enhances the TC owing to the reduced phonon scaterring at the filler-filler interfaces.[32, 35, 47-52]

3.6 Density

Figure 6a shows the density variations of the composites as a function of BNNSs loading and VE percentage. With increasing filler loading, the density for all the samples increases linearly. For example, the density of the composites increases from 1.1 to 1.2 g/cm^3 for the solid samples containing 10 wt% and 27.5 wt% BNNSs, respectively. The excellent linear relationship between the density and filler loading suggests that the BNNSs were homogeneously dispersed into the aqueous suspension without precipitation during foaming process. The density of the foamed composites is remarkably lower than that of solid samples because of the introduced air into the composites. Furthermore, the density of the foamed composites decreases with VE percentage under the same filler loading. The inset in **Figure 6**a displays the ultralight weight foam with 25 wt% BNNSs standing on a piece of tender leaf. For aeronautics and aerospace applications, materials with lightweight are a prerequisite to achieve high flying speed and save energy, so, the concurrently enhanced lightweight and TC performances of the porous BNNSs/c-PS composites' promotes future aerospace and avionic devices' heat dissipation.

Figure 6b demonstrates the effect of VE on the density and the TC of the composite foam containing 25 wt% BNNSs. It can be seen that, with the increase in VE, density reduces accordingly, and the TC first decreases due to the introduction of air into the composites, then increases to the maximum value before it decreases again. The maximum TC value further confirm that the biaxial strain-induced filler alignment along cell walls is strong enough to form the interconnected networks of filler in the foam and significantly promote the TC. Moreover, the sample with the maximum TC possesses a lower density and a smaller VE compared to the solid sample. Therefore, it is concluded that the lightweight polymer composites with a high TC can be obtained by using the foaming technology.[54]

3.7 Specific thermal conductivity

For polymer composites with potential applications in aviation and aerospace, effective weight reduction is highly desired because the weight reduction can significantly increase the flying speed and distance for aircraft and space rocket. In order to precisely describe the TC of foamed polymer composites, similar to specific strength, specific modulus and specific heat capacity, a new parameter, specific thermal conductivity (STC), i.e., TC divided by density, is suggested herein:

$$STC = \kappa / \rho \quad (4)$$

where, k is TC, and ρ is density.

Figure 6(c-d) illustrates the STC of the composites with various filler loadings and VE. From **Figure 6**c, it can be found that at low filler loadings the STC of the foamed polymers is lower than those of solid samples, whereas at higher filler loadings the foamed composites exhibit a much high STC compared with solid samples. As shown in **Figure 6**d, the STC curves exhibit a mount-shape against VE. At relatively low VE values, the STC increases to the maximum value, and then reduces slowly with increasing VE. Compared with solid samples, the STC of the foamed composites with higher filler loadings are much higher owing to their lower densities. However, at low filler loadings, the VE has less significant influence on the STC due to the absence of 3D network of fillers in the composites.[26-30] Therefore, in this study, at relatively low filler loadings, we successfully prepared polymer composites with much high STC compared with their solid counterparts at the same filler loading.

This kind of ultralight structures with 3D interconnected porous is propular in nature. For example, **Figure S4** (supporting information) shows the 3D interconnected porous structures of a loofah sponge after removal of seeds. In this work, the BNNSs/*c*-PS porous structure, silimar to the 3D interconnected loofah sponge structure, has the following advantages: 1) ultralight; 2) high

specific strength and modulus; 3) high STC, which are highly desired in the applications of aerospace and aircraft components.

In order to demonstrate the effectiveness and superiority of the foaming-induced filler network in enhancing the TC of the composites, the STC of this composite foams has been compared with the literature results as shown in **Figure 6**e.[2-4, 7-9, 12, 19-4, 26-30, 32-45,50-54] Compared to the literature reports on the thermally conductive polymer composites, the BNNSs/*c*-PS foam gives the best STC value at low filler loadings. **Figure 6**f summarizes the enhancement of the TC (*i.e.*, the TC ratio of composites vs. a polymer matrix) of the composites that have been reported.[2-4, 7-9, 12, 19-4, 26-30, 32-45,50-54] Clearly, the BNNSs/*c*-PS foam exhibits the highest TC enhancement at low weight fractions among the reported heat conductive composites.

3.8 Dielectric properties

Figure 7(a-b) presents the relative dielectric constants (ε) and loss versus VE percentage for the 30 wt% BNNSs/*c*-PS composites across the frequency range from 200 to 2×10^6 Hz. It can be seen that ε of the composites decreases with the increase of VE. The decrease in ε can be explained by the introduction of air in the composites as a result of very low ε of air.[35] Furthermore, ε for all the samples are apparently independent on frequency over the entire frequency range, suggesting that dipole polarization is the dominant mechanism and follows well with the external electric field.[1] **Figure S5** (supporting information) presents the ε and loss of the 20 wt% BNNSs/*c*-PS. The ε of the composites exhibits a very slight increase when the filler loading increases from 20 to 30 wt%. The loss decreases obviously due to the incorporation of air into the composites. Over the investigated frequency range, the loss is essentially lower than 0.005 for the two composites with various VE values.

Figure 7c presents the effective relative ε versus filler loading of the BNNSs/*c*-PS composites

with a VE of 92%. As the filler concentration increases, the effective relative ε increases slowly, and exhibits independent of frequency over the entire 200~2×10^6 Hz range. The effective relative ε of the composites with 20 and 30 wt% BNNSs only increases from 1.6 to 1.82 at 1 kHz, respectively, as compared to 2.8 and 3.1 of their solid counterparts. As seen in **Figure 7**d, the BNNSs/*c*-PS composites with a VE of 92% also show very low loss over the frequency range.

Figure 8(a-b) presents the effective relative ε and loss at 1 kHz versus temperature of the BNNSs/*c*-PS composites with a VE of 92%. ε for pure *c*-PS and three composites increases with the filler loading and rises very slowly with temperature. Only the composites with 30 wt.% BNNSs has a noticeable increase in ε starting at about 110 ^{o}C. As seen in **Figure 8**b, the loss also increases with filler loading, and increases slowly with temperature at <110 ^{o}C. After 110 ^{o}C, a abrupt increase of the loss to the maximum value is observed for all the composites, suggesting that the temperature plays a key role in determining the dielectric loss of the composites. This transition temperature actually corresponds to the glass transition temperature (T_g) of the *c*-PS. At a temperature near T_g, the dipoles begin to have enough mobility to contribute to the loss and ε.[44]

Figure 7(c-d) shows the effective relative ε and loss versus temperature of the 20 wt% BNNSs/*c*-PS composites with various VE. With the increase of VE, all the composites exhibit an obvious decrease in ε and loss. All the ε are almost independent on temperature from room temperature to 180 ^{o}C, whereas the loss increases with temperature and exhibits a clear rise starting from T_g owing to the enhanced mobility of polymer segments at elevated temperatures.[55] It can be seen that compared with pure *c*-PS and the solid BNNSs/*c*-PS with the same filler loading, the foamed composites still exhibit very low ε and loss from room temperature to 180 ^{o}C as shown in **Figure S6** (supporting information).

4 Conclusion

In summary, *c*-PS foams with various BNNSs loadings at different VE percents were prepared and characterized to investigate the effects of foam morphologies on the TC and dielectric properties of the formed composites. It is found that the VE has a dramatical effect on the TC of the composite foam. The optimized VE gives the composite foam with a higher TCs than their solid counterparts. The biaxial stress field yielded durining the form formation promotes BNNSs alignment along the cell wall and the formation of 3D interconnected fillers in the foams at the optimized VE, thereby leading to much enhanced TC. For example, the TC of 30 wt% of BNNSs/*c*-PS composites with a VE of 45% reach as high as 1.28 W/m K, which represents a 97% increases over 0.65 W/m K of its solid counterpart.

In contrast, at low VE, the foams exhibit low TC owing to the absence of interconnected network of fillers in the matrix and the introduction of thermally insulating air voids into the composites. High VE percentage would not only result in high volume fraction of thermally insulating air voids but also disrupt the development of continuous thermally conductive path, leading to decreased TC. The experimental data are consistent with the simulation results.

Furthermore, the composite foams exhibit ultralow density, ε and loss at wide frequency and temperature ranges, along with ultrahigh STC. In summary, the results demonstrate that the foaming-assisted filler networking is a feasible processing strategy to improve the TC of the composite foams especially at low filler loadings. The polymer composite foams with low ε and loss and ultrahigh STC could provide a new material family for potential applications in aeronautics and aerospace to address the emerging needs of thermal managements.

Supporting Inforation

Schematic representation of the effects of VE and filler loading on the TC of foamed polymers

(**Figure S1**); Effect of particle size on TC for foamed composites with various VE and filler loadings (**Figure S2**); Effect of cell size on TC of foamed composites with various VE and filler loadings (**Figure S3**); 3D interconnected biological porous structures found in the nature loofah sponge (**Figure S4.**); Dielectric properties of the 20 wt% BNNSs/*c*-PS composites as a function of VE (**Figure S5.**); Dielectric properties of *c*-PS and BNNSs/*c*-PS composites as a function of VE (**Figure S6.**) (PDF)

AUTHOR INFORMATION

Corresponding Author

*E-mail: wang@matse.psu.edu

ORCID

Wenying Zhou: 0000-0001-6481-2604

Yong Zhang: 0000-0002-6478-6167

He Li: 0000-0002-4076-7279

Wenhan Xu: 0000-0002-4347-2601

Longqing Chen: 0000-00003-2050-5383

Qing Wang: 0000-0002-5968-3235

Notes

The authors declare no competing financial interest.

Acknowledgements

Dr. Wenying Zhou gratefully acknowledges the financial supports from the National Natural

Science Foundation of China (51937007, 51577154), the Key Laboratory of Engineering Dielectrics and Its Application, Ministry of Education, Harbin University of Science and Technology (KF20151111), and the fellowship provided by the China Scholarship Council (CSC, 201608610027).

REFERENCES

(1) Chen, H. Y.; Ginzburg, V. V.; Yang, J; Yang, Y. F.; Liu, W.; Huang, Y.; Du, L. B.; Chen, B. Thermal Conductivity of Polymer-based Composites: Fundamentals and Applications. *Prog. Polym. Sci*. **2016**, 59, 41-85.

(2) Du, B. X.; Cui, B. Effects of Thermal Conductivity on Dielectric Breakdown of Micro, Nano Sized BN Filled Polypropylene Composites. *IEEE Trans. Dielectr. Electr. Insul*. **2016**, 23, 2116-2125.

(3) Zhou, Y.; Hu, J.; Chen, X.; Yu, F.; H, J. L. Thermoplastic Polypropylene/Aluminum Nitride Nanocomposites with Enhanced Thermal Conductivity and Low Dielectric Loss. *IEEE Trans. Dielectr. Electr. Insul*. **2016**, 23, 2768-2776.

(4) Yang, Y.; Huang, X. P.; Cao, Z. Y.; Chen, G. Thermally Conductive Separator with Hierarchical Nano/Microstructures for Improving Thermal Management of Batteries. *Nano Energy*. **2016**, 22, 301-309.

(5) Li, Q.; Chen, L.; Gadinski, M. R.; Zhang, S.; Zhang, G.; Lagodkine,U. Li.; Haque, A.; Chen, L. Q.; Jackson, N.; Wang, Q. Flexible High-temperature Dielectric Materials from Polymer Nanocomposites. *Nature*. **2015**, 523, 576-579.

(6) Bozlar, M.; He, D. L.; Bai, J. B.; Chalopin, Y.; Mingo, N.; Volz, S. Carbon Nanotube Microarchitectures for Enhanced Thermal Conduction at Ultra Low Mass Fraction on in Polymer Composites. *Adv. Mater*. **2010**, 22, 1654-1658.

(7) Kazem, N.; Bartlett, M. D.; Powell-Palm, M. J.; Huang, X. N.; Sun, W. H.; Malen, J. A.; Majidi, C. High Thermal Conductivity in Soft Elastomers with Elongated Liquid Metal Inclusions. *P. Natl. Acad. Sci.*

USA. **2017**,114, 2143-2148.

(8) Jeong, S. H.; Chen, S.; Huo, J. X.; Gamstedt, E. K.; Liu, J.; Zhang, S. L.; Zhang, Z. B.; Hjort, K.; Wu, Z. G. Mechanically Stretchable and Electrically Insulating Thermal Elastomer Composite by Liquid Alloy Droplet Embedment. *Sci. Rep.* **2015**, 5, 18257-18266.

(9) Zhao, S. A.; Chang, H. Y.; Chen, S. J.; Cui, J.; Yan, Y. H. High-performance and Multifunctional EEpoxy Composites Filled with Epoxide-functionalized Graphene. *Euro. Polym. J*. **2016**, 84, 300-312.

(10) Lee, S. H.; Jung, J. H.; Oh, I. K. 3D Networked Grapheme Ferromagnetic Hybrids for Fast Shape Memory Polymers with Enhanced Mechanical Stiffness and Thermal Conductivity. *Small.* **2014**, 10, 3880-3886.

(11) Yao, Y. M.; Zeng, X. L.; Wang, F. F.; Sun, R.; Xu, J. B.; Wong, C. P. Significant Enhancement of Thermal Conductivity in Bioinspired Freestanding Boron Nitride Papers Filled with Graphene Oxide. *Chem. Mater.* **2016**, 28, 1049-1057.

(12) Feng, C. P.; Ni, H. Y.; Chen, J.; Yang, W. Facile Method to Fabricate Highly Thermally Conductive Graphite/PP Composite with Network Structures. *ACS Appl. Mater. Inter.* **2016**, 8, 19732-19738.

(13) Shen, S.; Henry, A.; Tong, J. K.; Zheng, R. T; Chen, G. Polyethylene Nanofibres with Very High Thermal Conductivities. *Nat. Nanotechnol.* **2010**, 5, 251-255.

(14) Singh, V.; Bougher, T. L.; Weathers, A.; Cai, Y.; Bi, K. D.; Pettes, M. T.; Stames, S. M.; Lv, W.; Resler, D. P.; Gattuso, T. R.; Altmsn, D. H.; Sandhage, K. H.; Shi, L.; Henry, A.; Cola, B. A. High Thermal Conductivity of Chain-oriented Amorphous Polythiophene. *Nat. Nanotechnol.* **2014**, 9, 384-390.

(15) Regner, K. T.; Sellan, D. P.; Su, Z. H.; Amon, C. H.; McGaughey, A. J. H.; Malen, J. A. Broadband Phonon Mean Free Path Contributions to Thermal Conductivity Measured Using Frequency Domain Thermoreflectance. *Nat. Commun.* **2013**, 4, 1640-1646.

(16) Zhong, Z. X.; Wingert, M. C.; Strzalka, J.; Wang, H.; Sun, T.; Wang, J.; Chen, R. K.; Jiang, Z. Structure-induced Enhancement of Thermal Conductivities in Electrospun Polymer Nanofibers. *Nanoscale*. **2014**,

6, 8283-8291.

(17) Zeng, X. L.; Yao, Y. M.; Gong, Z. Y.; Wang, F. F.; Sun, R.; Xu, J. B.; Wong, C. P. Ice-templated Assembly Strategy to Construct 3D Boron Nitride Nanosheet Networks in Polymer Composites For Thermal Conductivity Improvement. *Small.* **2015**, 11, 6205-6213.

(18) Zeng, X. L.; Ye, L.; Yu, S. H.; Sun, R.; Xu, J. B.; Wong, C. P. Facile Preparation of Superelastic and Ultralow Dielectric Boron Nitride Nanosheet Aerogels Via Freeze-casting Process. *Chem. Mater.* **2015**, 27, 5849-5855.

(19) Anithambigai, P.; Mutharasu, D.; Huong, L. H.; Zahner, T.; Laceyet, D. Synthesis and Thermal Analysis of Aluminium Nitride Filled Epoxy Composites and Its Effective Application as Thermal Interface Material for LED Applications. *J. Mater. Sci. Mater. El.* **2014**, 25, 4814-4821.

(20) Kim, K.; Kim, J. Magnetic Aligned AlN/epoxy Composite for Thermal Conductivity Enhancement at Low Filler Content. *Compos. Part B-Eng*. **2016**, 93, 67-74.

(21)Wu,S. Y.; Huang, Y. L.; Ma, C. M.; Yuen, S. M.; Teng, C. C.; Yang, S. Y. Mechanical, Thermal and Electrical Properties of Aluminum Nitride/ polyetherimide Composites. *Compos. Part A.* **2011**, 42, 1573-1583.

(22) Choi, S.; Kim, J. Thermal Conductivity of Epoxy Composites with A Binary-particle System of Aluminum Oxide and Aluminum Nitride Fillers. *Compos. Part B.* **2013**, 51, 140-147.

(23) Takahashi, S.; Imai, Y.; Kan, A.; Hotta, Y.; Ogawa, H. Dielectric and Thermal Properties of Isotactic Polypropylene/hexagonal Boron Nitride Composites for High-frequency Applications. *J. Alloy. Compd.* **2014**, 615, 141-145.

(24) Bigg, D. Thermal Conductivity of Heterophase Polymer Compositions. *Adv. Polym. Sci*. **1995**, 119, 1-30.

(25) Mu, M.; Wan, C.; Mcnally, T.; Thermal Conductivity of 2D Nano-structured Graphitic Materials and Their Composites with Epoxy Resins. *2D Mater.* **2017**, 4, 042001-042023.

(26) Mu, L. W.; Ji, T.; Chen, L.; Mehra, N.; Shi, Y. J.; Zhu, J. H. Paving the Thermal Highway with

Self-organized Nanocrystals in Transparent Polymer Composites. *ACS Appl. Mater. Interfaces.* **2016**, 8, 29080-29087.

(27) Wang, J. W.; Li, H. R.; Li, G. H.; Liu, Z. X.; Zhang, Q. X.; Wang, N. Y.; Qu, X. W. Noncovalent Functionalization of Boron Nitride and Its Effect on the Thermal Conductivity of Polycarbonate Composites. *J. Appl. Polym. Sci*. **2017**, 134,44978-44986.

(28) Fang, H.; Bai, S. L. Wong, C. P.; Thermal, Mechanical and Dielectric Properties of Flexible BN Foam and BN Nanosheets Reinforced Polymer Composites for Electronic Packaging Application. *Compos. Part A-Appl. S.* **2017**, 100, 71-80.

(29) Kim, K.; Ju, H.; Kim, J. Vertical Particle Alignment of Boron Nitride and Silicon Carbide Binary Filler System for Thermal Conductivity Enhancement. *Compos. Sci. Technol*. **2016**, 123, 99-105.

(30) Cho, H. B.; Nakayama,T.; Suematsu, H.; Suzuki, T.; Jiang, W. H.; Niihara, K.; Song, E.; Eom, N. S. A.; Kim, S.; Choa, Y. H. Insulating Polymer Nanocomposites with High-thermal-conduction Routes Via Linear Densely Packed Boron Nitride Nanosheets. *Compos. Sci. Technol.* **2016**, 129, 205-213.

(31) Ding, H.; Guo, Y.; Leung, S. N. Development of Thermally Conductive Polymer Matrix Composites by Foaming- assisted Networking of Micron- and Submicron-scale Hexagonal Boron Nitride. *J. Appl. Polym. Sci.* **2015**, 133(4): -.

(32) Zhang, J.; Wang, X. N.; Yu, C. P.; Li, Q. L.; Li, Z.; Li, C. W.; Lu, H. F.; Zhang, Q. C.; Zhao, J. X.; Hu, M.; Yao, Y. G. A Facile Method to Prepare Flexible Boron Nitride/poly(vinyl alcohol) Composites with Enhanced Thermal Conductivity. *Compos. Sci. Technol.* **2017**, 149, 41-47.

(33) Kim, K.; Kim, J.; Vertical Filler Alignment of Boron Nitride/epoxy Composite for thermal Conductivity Enhancement Via external Magnetic Field. *Inter. J. Therm. Sci*. **2016**, 100, 29-36.

(34) Chen, J.; Huang, X. Y.; Zhu, Y. K.; Jiang, P. K. Cellulose Nanofiber Supported 3D Interconnected BN Nanosheets for Epoxy Nnanocomposites with Ultrahight Thermal Management Capability. *Adv. Mater*. **2017**, 27,

1604754-1604762.

(35) Sun, W.; Wang, L.; Yang, Z.; Zhu, T. Z.; Wu, T. T.; Dong, C.; Liu, G. C. Tuning the Oxidation Degree of Graphite Toward Highly Thermally Conductive Graphite/epoxy Composites. *Chem. Mater*. **2018**, 30, 7473-7483.

(36) Wu, K.; Liao, P.; Du, R.; Zhang, Q.; Chen, F.; Fu, Q. Preparation of A Thermally Conductive Biodegradable Cellulose Nanofiber/hydroxylated Boron Nitride Nanosheet Film: the Critical Role of Edge-hydroxylation. *J. Mater. Chem A*. **2018**, 6, 11863-11873.

(37) Xu, Y.; Kraemer, D.; Song, B.; Jiang, Z.; Zhou, J. W.; Loomis, J.; Wang, J. J.; Li, M. D.; Ghasemi, H.; Huang, X. P.; Li, X. B.; Chen, G. Nanostructured Polymer Films with Metal-like Thermal Conductivity. *Nat. Commun.* **2019**, 10, 1771-1778.

(38) Li, X. H.; Liu, P.; Li, X.; An, F.; Min, P.; Liao, K. N.; Yu, Z. Z. Vertically Aligned, Ultralight and Highly Compressive All-graphitized Graphene Aerogels for Highly Thermally Conductive Polymer Composites. *Carbon*. **2018**, 140, 624-633.

(39) Li, X.; Feng, Y.; Chen, C.; Ye, Y. S.; Zeng, H. X.; Qu, H.; Liu, J. W.; Zhou, X. P.; Long, S. J.; Xie, X. L. Highly Thermally Conductive Flame Retardant Epoxy Nanocomposites with Multifunctional Ionic Liquid Flame Retardant-functionalized Boron Nitride Nanosheets. *J. Mater. Chem A*. **2018**, 6, 20500-20512.

(40) Saeidijavash, M.; Garg, J.; Grady, B.;Smith, B.; Li, Z. L.; Young, R. J.; Tarannum, F.; Bekri, N. B. High Thermal Conductivity Through Simultaneously Aligned Polyethylene Lamellae and Graphene Nanoplatelets. *Nanoscale*. **2017**, 9, 12867-12873.

(41) Su, Z.; Wang, H.; Tian, K.; Huang, W. Q.; Xiao, C.; Guo, Y. L.; He, J.; Tian, X. Y. The Combination of π-π Interaction And Covalent Bonding Can Synergistically Strengthen the Flexible Electrical Insulating Nanocomposites with Well Adhesive Properties and Thermal Conductivity. *Compos. Sci. Technol*. **2018**, 155, 1-10.

(42) Fu, C.; Li, Q.; Lu, J.; Mateti, S.; Cai, Q. R.; Zeng, X. L.; Du, G. P.; Sun, R.; Chen, Y.; Xu, J. B.; Wong, C. P.

Improving Thermal Conductivity of Polymer Composites by Reducing Interfacial Thermal Resistance Between Boron Nitride Nanotubes. *Compos. Sci. Technol*. **2018**, 165, 322-330.

(43) Zhang, J.; Li, C. W.; Yu, C. P.; Wang, X. N.; Li, Q. L.; Lu, H. F.; Zhang, Q. C.; Zhao, J. X.; Songfeng, E.; Hu, M.; Yao, Y. G. Large Improvement of Thermal Transport and Mechanical Performance of Polyvinyl Alcohol Composites Based on Interface Enhanced by SiO_2 Nanoparticle-modified-hexagonal Boron Nitride. *Compos. Sci. Technol*. **2019**, 169, 167-175.

(44) Vu, M. C.; Tran, T. S.; Bae, Y. H.; Yu, M. J.; Doan, V. C.; Lee, J. H.; An, T. K.; Kim, S. R. Self-Assembly of Carbon Nanotubes and Boron Nitride via Electrostatic Interaction for Epoxy Composites of High Thermal Conductivity and Electrical Resistivity. *Macromol. Res.* **2018**, 26, 521-528.

(45) Xu, S.; Liu, H.; Li, Q. M.; Mu, Q. W.; Wen, H. Y. Influence of Magnetic Alignment and Layered Structure of BN&Fe/EP on Thermal Conducting Performance. *J. Mater. Chem. C*. **2016**, 4, 872-878.

(46) Han, J. K.; Du, G. L.; Gao, W. W.; Bai, H. An Anisotropically High Thermal Conductive Boron Nitride/Epoxy Composite Based on Nacre-Mimetic 3D Network. *Adv. Funct. Mater*. **2019**, 29, 1900412-1900421

(47) Hong, H.; Jung, Y. H.; Lee, J. S.; Jeong, C.; Kim, J. U.; Lee, S.; Ryu, H.; Kim, H.; Ma, Z. Q.; Kim, T. Anisotropic Thermal Conductive Composite by the Guided Assembly of Boron Nitride Nanosheets for Flexible and Stretchable Electronics. *Adv. Funct. Mater*. **2019**, 29, 1902575-1902583..

(48) Zhou, H. J.; Deng, H.; Zhang, L.; Fu, Q. Significant Enhancement of Thermal Conductivity in Polymer Composite via Constructing Macroscopic Segregated Filler Networks. *ACS Appl. Mater. Interfaces*. **2017**, 9, 34, 29071–29081.

(49) Shi, A.; Li, Y.; Liu, W.; Xu, J. Z.; Yan, D. X.; Lei, J.; Li, Z. M. Highly Thermally Conductive and Mechanically Robust Composite of Linear Ultrahigh Molecular Weight Polyethylene and Boron Nitride Via Constructing Nacre-like Structure. *Compos. Sci. Technol*. **2019**, 184, 107858-107864.

(50) Woltornist, S. J.; Varghese, D.; Massucci, D.; Cao, Z.; Dobrynin, A. V.; Adamson, D. H. Controlled 3D

Assembly of Graphene Sheets to Build Conductive, Chemically Selective and Shape-Responsive Materials. *Adv. Mater*. **2017**, 29, 1064947-1064952.

(51) Okamoto, M.; Nam, P. H.; Maiti, P.; Kotata, T.; Nakayama, T.; Takada, M.; Ohshima, M.; Usuki, A.; Hasegawa, N.; Okamoto, H. Biaxial Flow-induced Alignment of Silicate Layers in Polypropylene/clay Nanocomposite Foam. *Nano Lett*. **2001**, 1, 503-505.

(52) Yan, D. X.; Dai, K.; Xiang, Z. D.; Li, Z. M.; Ji, X.; Zhang, W. Q. Electrical Conductivity and Major Mechanical and Thermal Properties of Carbon Nanotube - filled Polyurethane Foams. *J. Appl. Polym. Sci*. **2011**, 120, 3014-3019.

(53) Guerra, V.; Wan, C.; Mcnally, T. Thermal Conductivity of 2D Nano-structured Boron Nitride (BN) and Its Composites with Polymers. *Prog. Mater Sci.* **2018**, 100, 170-186.

(54) Congliang, H.; Xin, Q.; Ronggui, Y. Thermal Conductivity of Polymers and Polymer Nanocomposites. *Mater. Sci. Eng., R.* **2018**, 132, 1-22.

(55) Kim, Y.; Kim, M.; Seong, H. G.; Jung, J. Y.; Baeck, S. H.; Shim, S. E. Roles of Silica-coated Layer on Graphite for Thermal Conductivity, Heat Dissipation, Thermal Stability, and Electrical Resistivity of Polymer Composites. *Polymer*. **2018**, 148, 295-302.

(56) Zhu, Z.; Li, C.; Songfeng, E.; Xie, L. Y.; Geng, R. J.; Lin, C. T.; Li, L. Q.; Yao, Y. G. Enhanced Thermal Conductivity of Polyurethane Composites Via Engineering Small/large Sizes Interconnected Boron Nitride Nanosheets. *Compos. Sci. Technol.* **2019**, 170, 93-100.

(57) Xu, Y.; Zhang, S.; Wang, P.; Wang, J. S. Synthesis of Poly (Butylene Succinate) Phosphorus-containing Ionomers for Versatile Crystallization and Improved Thermal Conductivity. *Polymer*. **2018**, 154, 258-271.

(58) Wang, J. J.; Wang, Y.; Ihlefeld, J. F.; Hopkins, P. E.; Chen, L. Q. Tunable Thermal Conductivity Via Domain Structure Engineering in Ferroelectric Thin Films: A Phase-field Simulation. *Acta Mater*. **2016**, 111, 220-231.

(59) Wang, J. J.; Ma, X. Q.; Li, Q.; Britson, J.; Chen, L. Q. Phase Transitions and Domain Structures of Ferroelectric Nanoparticles: Phase Field Model Incorporating Strong Elastic and Dielectric Inhomogeneity. *Acta Mater.* **2013**, 61, 7591-7603.

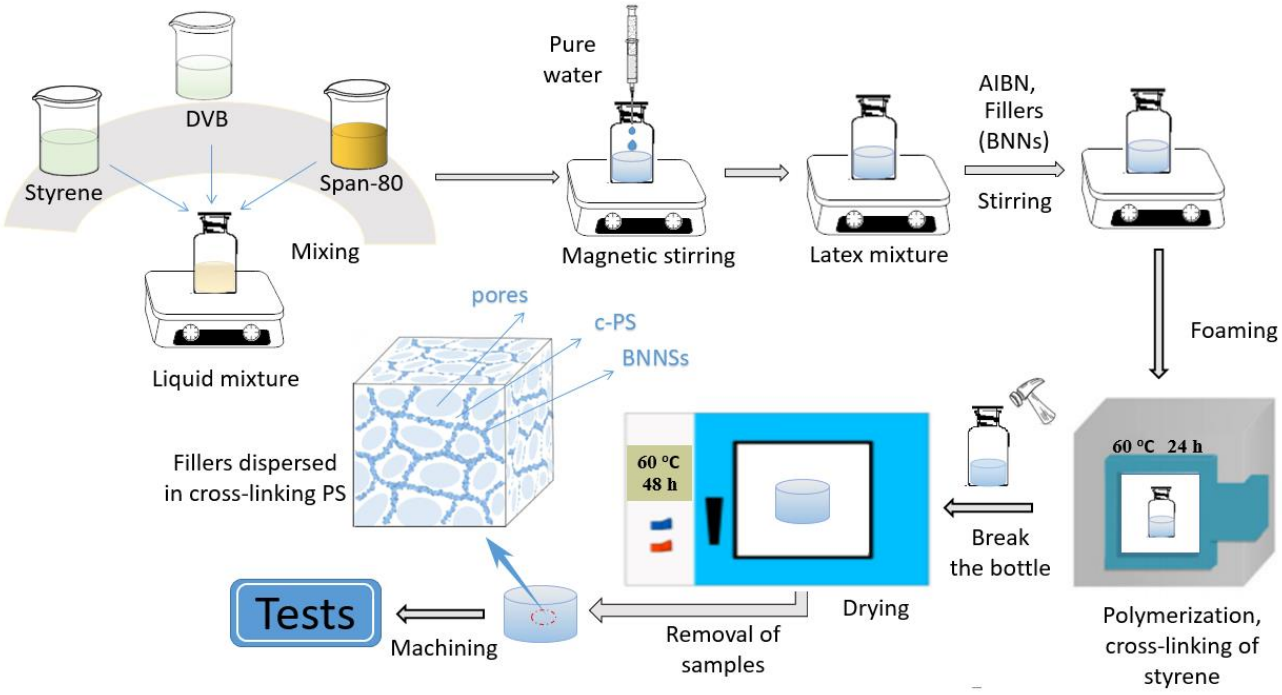

Figure 1. Schematic diagram of light porous cross-linking polystyrene with high thermal conductivity by constructing 3D interconnected network of boron nitride nanosheets.

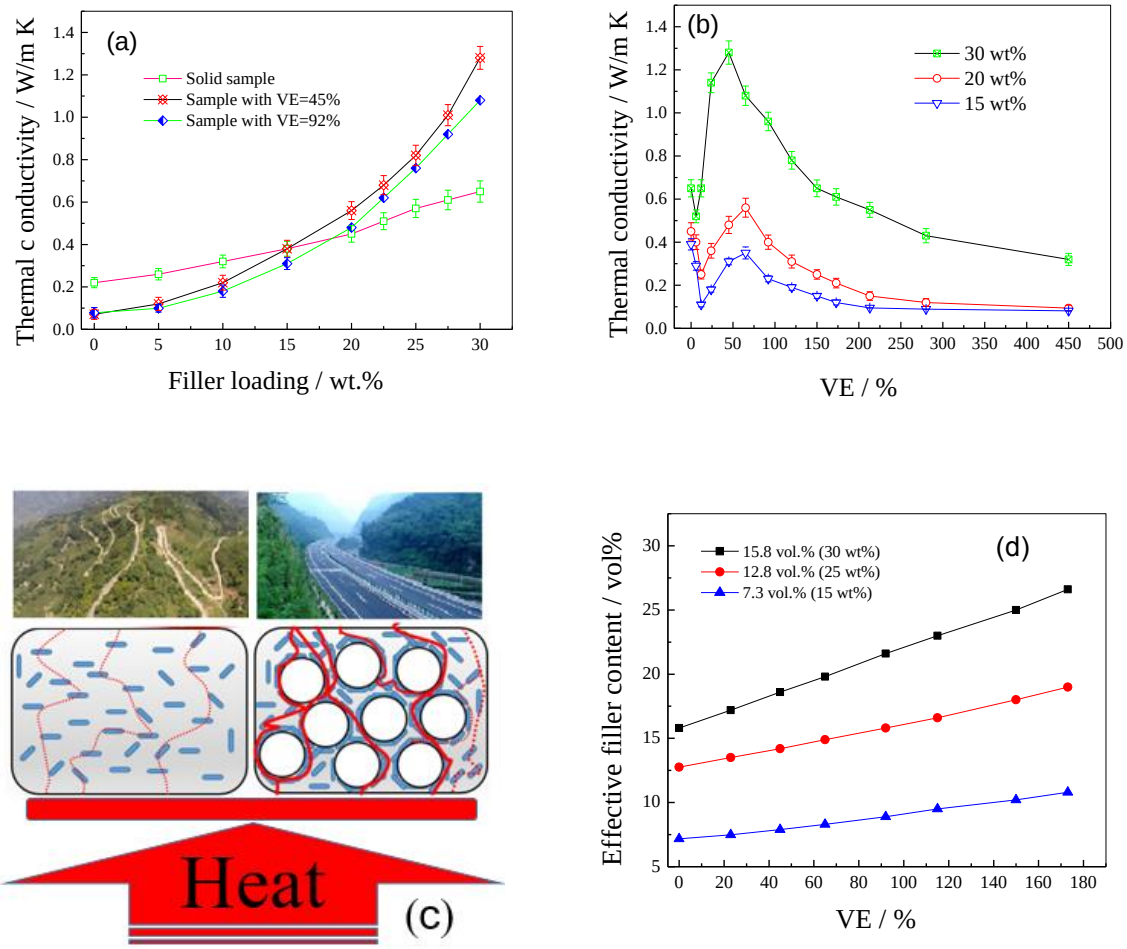

Figure 2. Dependence of TC of the composites on filler loading (a) and VE (b); Schematic representation of heat transfer in solid sample without heat conductive pathway, and foamed samples with heat conductive network of fillers (c); Effect of VE on effective filler loading for foamed composites (d).

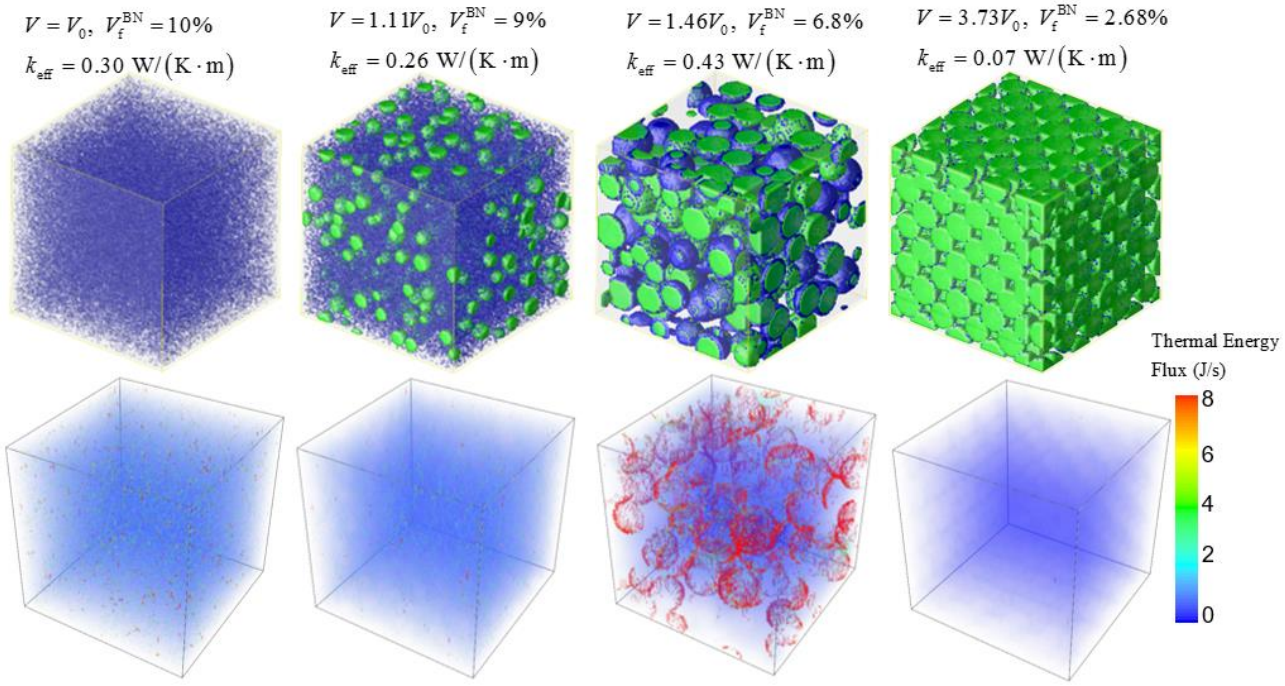

Figure 3. Microstructures (upper panel) and effective TC and energy flux distributions (lower panel) for the composites with different volume expansion ratios. In the microstructure, blue color and green color represent BNNSs phase and pore phase, respectively. The transparent space represents the polymer phase.

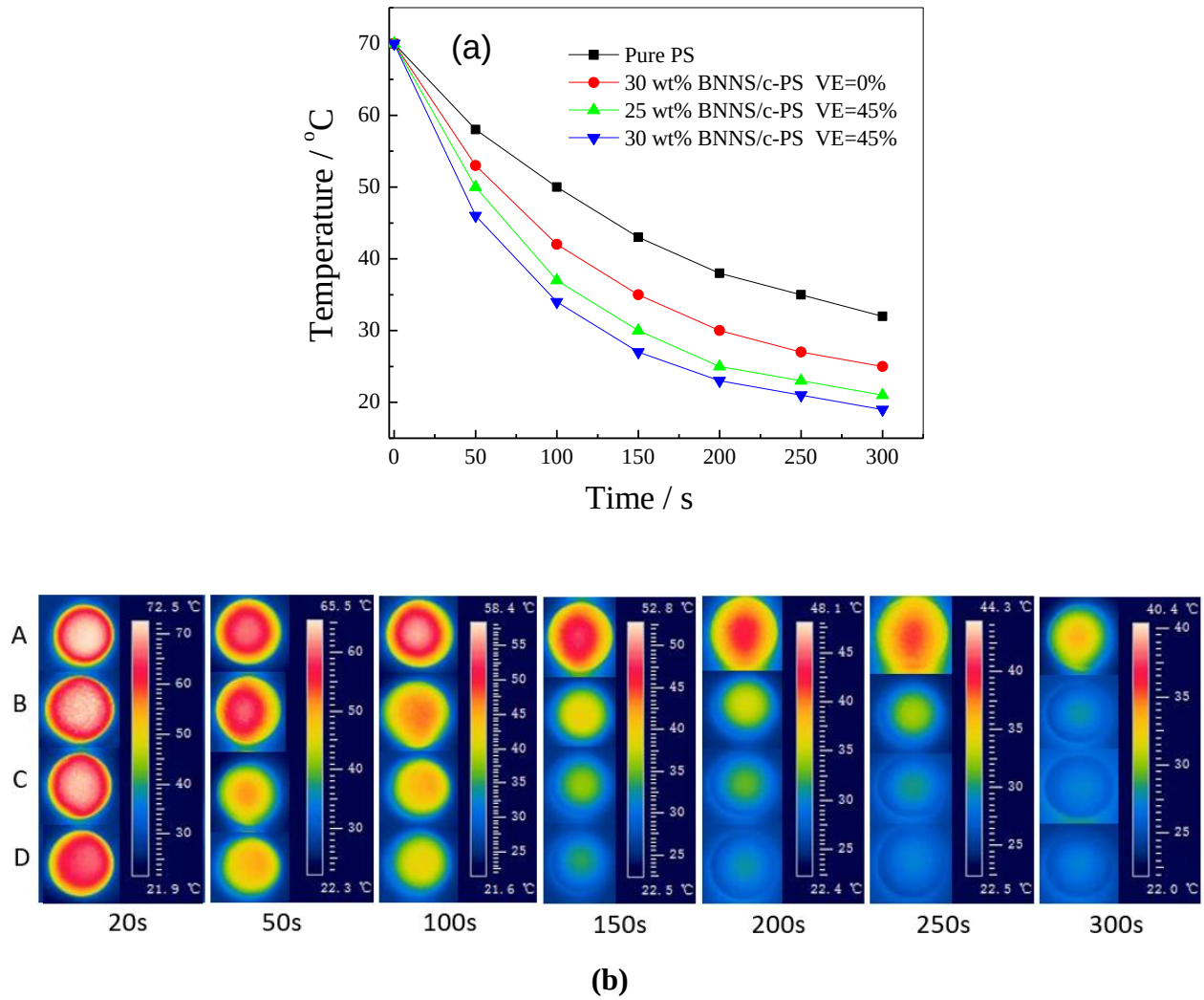

Figure 4. (a) Surface temperature variation with cooling time of pure c-PS (A), 30 wt% BNNSs/c-PS (VE=0) (B), 25 wt% BNNSs/c-PS (VE=45%) (C), and 30 wt% BNNSs/c-PS (VE=45%) (D); (b) Infrared thermal images of A, B, C and D at different times.

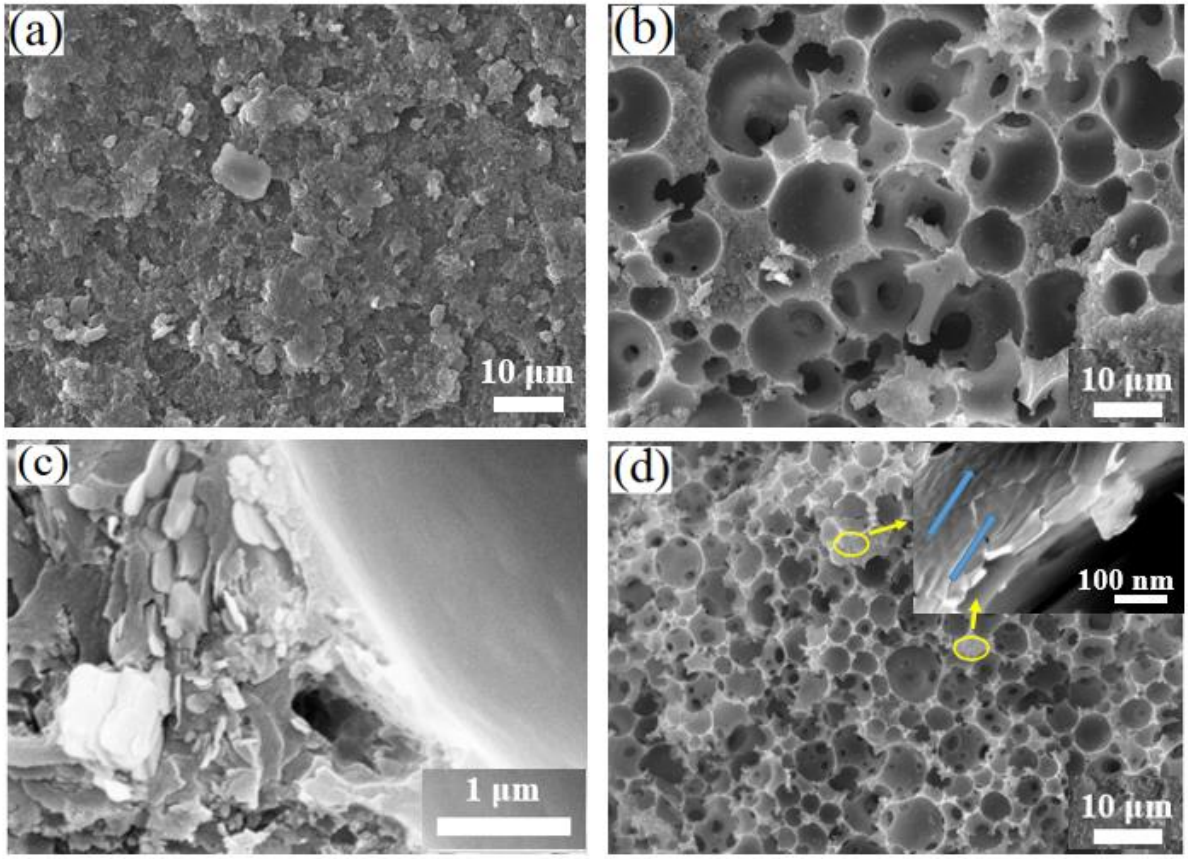

Figure 5. Micrographs of 30 wt% BNNSs/c-PS (VE=0%) (a), 25 wt% BNNSs/c-PS (VE=45%) (b-c), and 30 wt% BNNSs/c-PS (VE=45%) (d), the inset is the dispersion of BNNSs in c-PS matrix inside the cell wall.

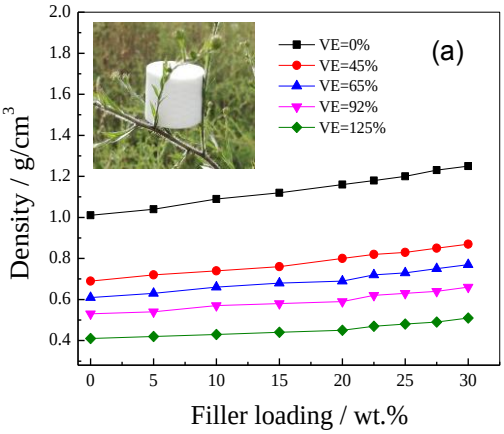

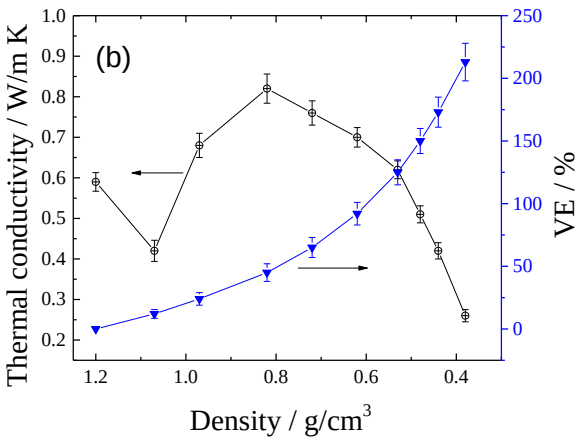

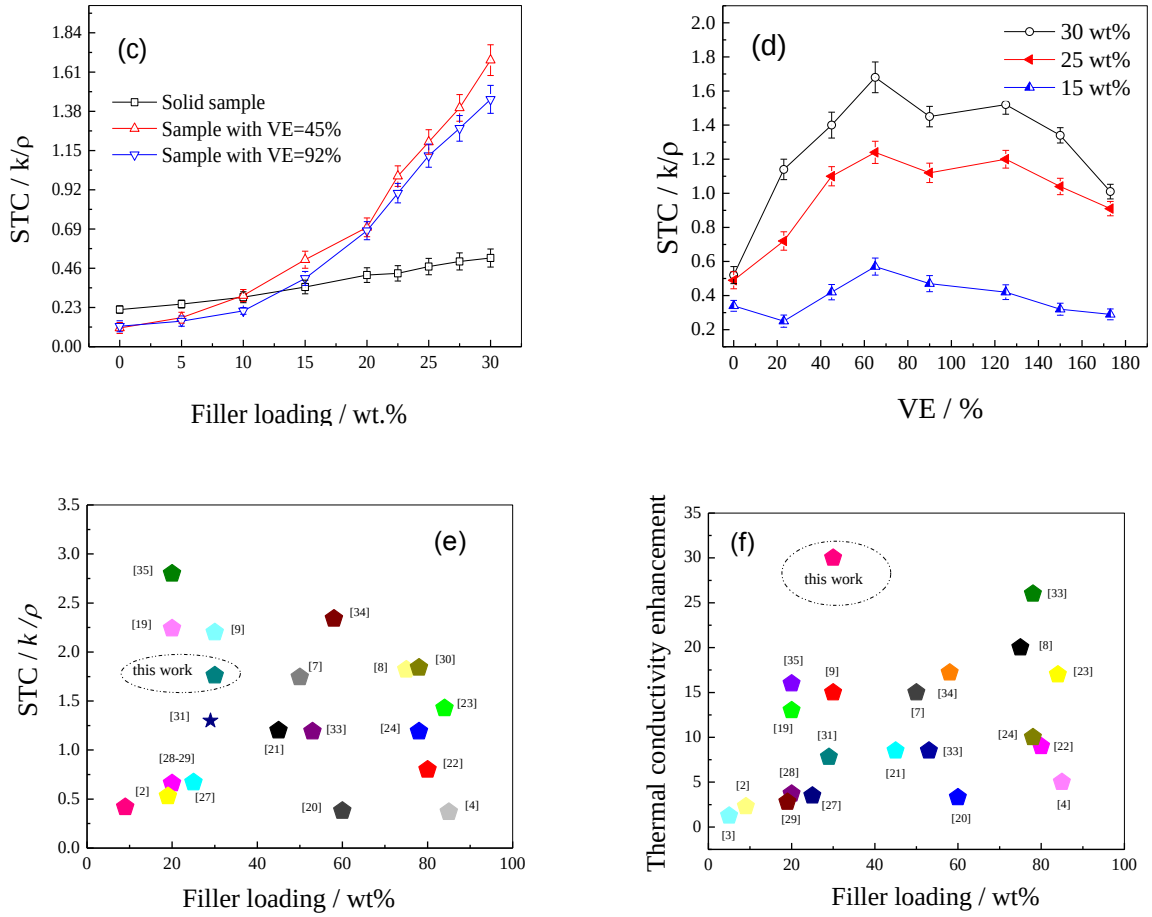

Figure 6. (a) Dependence of density of composite foams on VE, the inset photograph is a BNNSs/c-PS foam standing on a piece of tender branch, (b) Effects of VE on TC and density of composite foams with 25 wt% BNNSs, (c-d) STC as a function as filler loading and VE, (e) STC and (f) TC enhancement of composite foams and other composites in previous works.

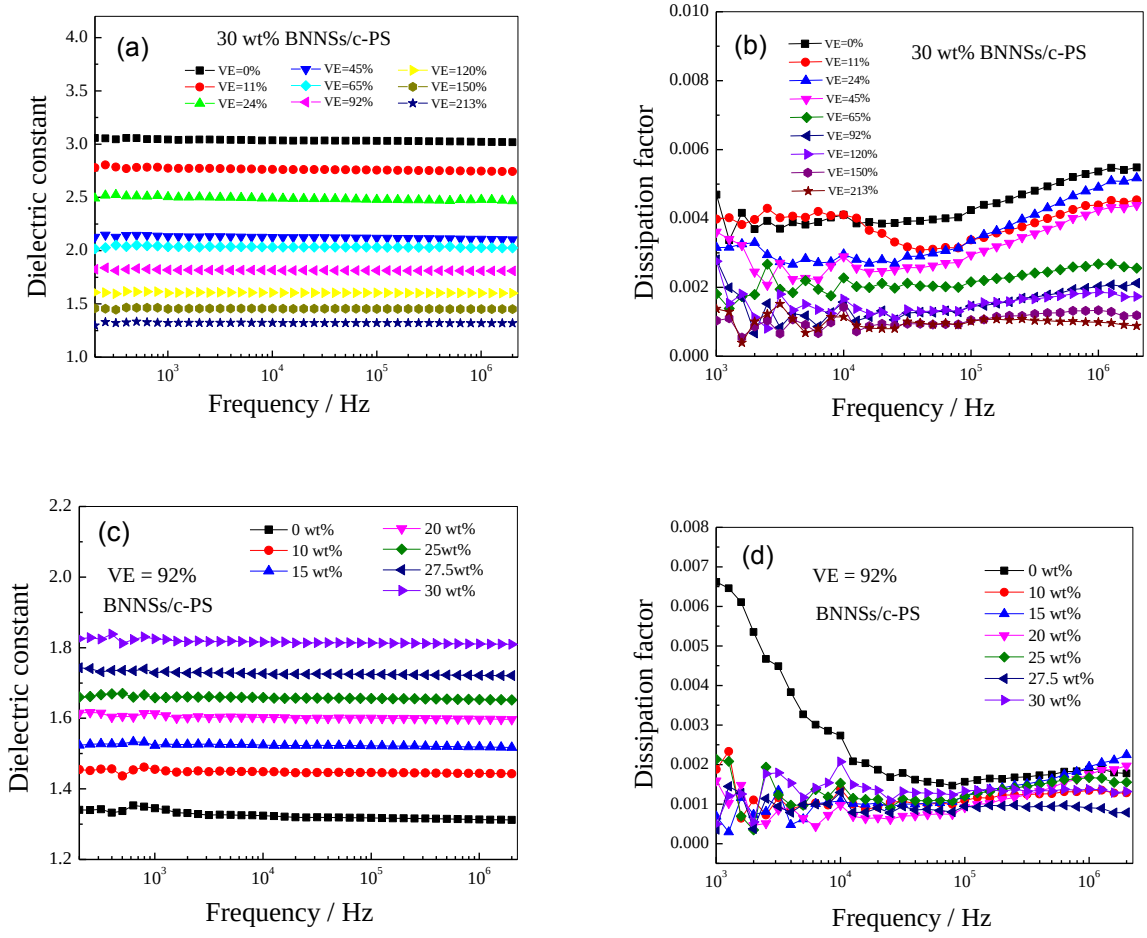

Figure 7. (a) dielectric permittivity and (b) dissipation factor of 30 wt% BNNSs/c-PS composites as a function of VE, (c) dielectric permittivity and (d) dissipation factor of BNNSs/c-PS composites with a VE of 92% as a function of filler loading.

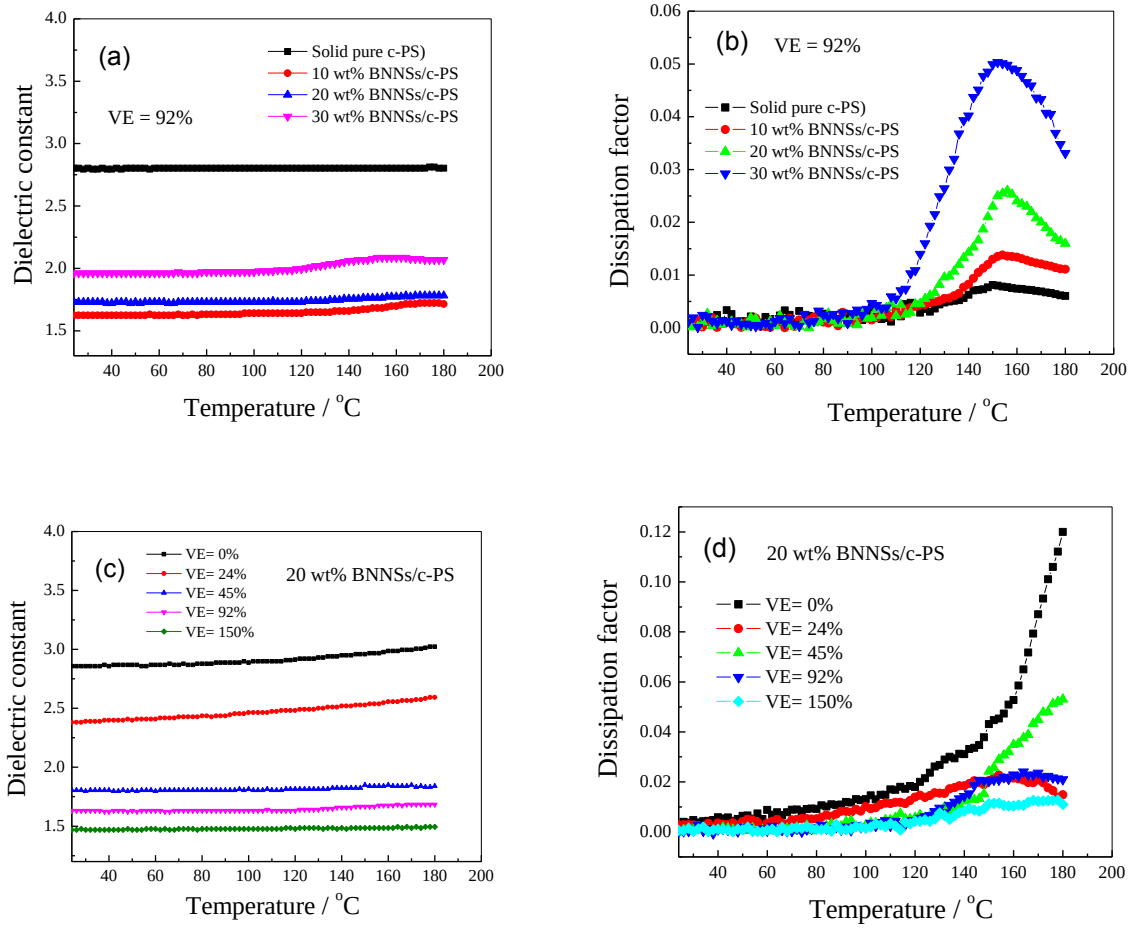

Figure 8. (a) dielectric permittivity and (b) dissipation factor (1000Hz) of c-PS composites with various loading of BNNSs at a VE of 92% as a function of filler loading, (c) dielectric permittivity and (d) dissipation factor (1000Hz) of 20 wt% BNNSs/c-PS composites as a function of VE.

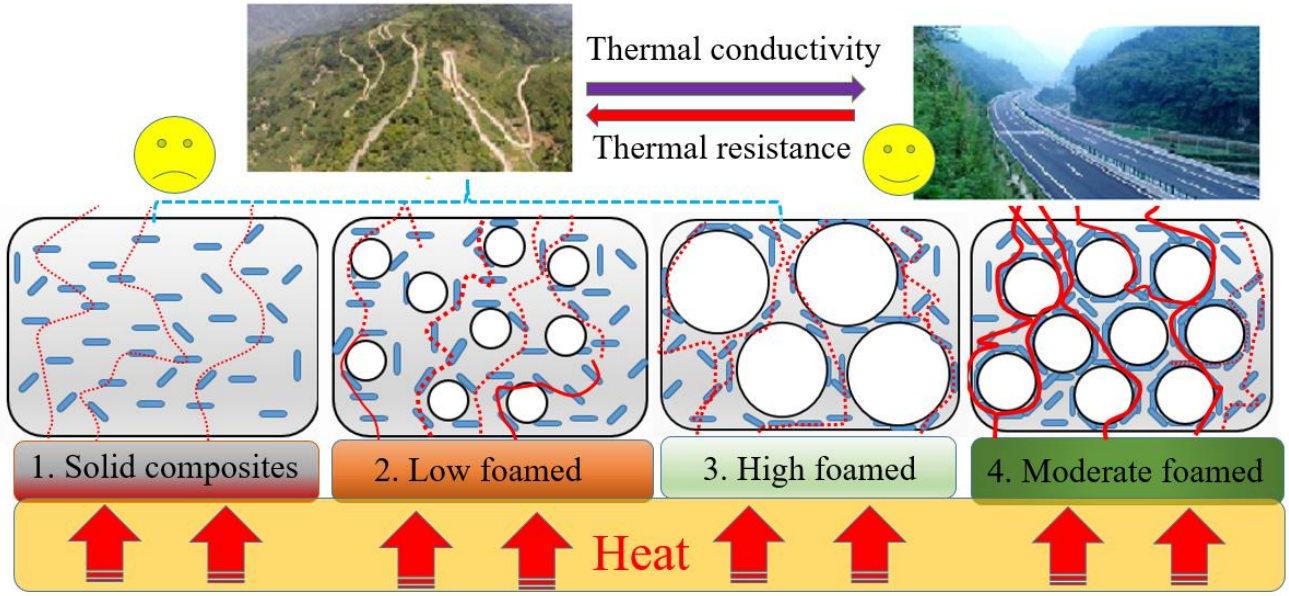
Thermal conductivity
Thermal resistance
1. Solid composites
2. Low foamed
3. High foamed
4. Moderate foamed
Heat